Nat. Hazards Earth Syst. Sci. Discuss., 3, 1113–1136, 2015
www.nat-hazards-earth-syst-sci-discuss.net/3/1113/2015/
doi:10.5194/nhessd-3-1113-2015

Natural Hazards and Earth System Sciences
Open Access
Discussions

Modelling of the hydrological connectivity changes in the Minjiang Upstream after the Wenchuan earthquake using satellite remote sensing and DEM data

H. Z. Zhang[1,2,3], **T. H. Chi**[1], **and J. R. Fan**[2]

[1]Institute of Remote Sensing and Digital Earth, Chines Academy of Sciences, Beijing, 100101, China
[2]Institute of Mountain Hazards and Environment, Chines Academy of Sciences, Chengdu, 610041, China
[3]University of Chinese Academy of Sciences, Chinese Academy of Sciences, Beijing, 100049, China

Received: 20 January 2015 – Accepted: 23 January 2015 – Published: 5 February 2015

Correspondence to: H. Z. Zhang (zhanghz@radi.ac.cn)

Published by Copernicus Publications on behalf of the European Geosciences Union.

Abstract

The 2008 Wenchuan earthquake-induced landslides destroyed larger areas of mountain vegetation and produced large volume of landslide-debris, which made the vegetation's hydrological adjusting function diminished and made the hydrological progresses in slopes changed, resulting in severe erosion and catastrophic debris flows for a rather long time. Since 2008, the landslide-damaged vegetation and its hydrological function have been recovering. In this paper, the Minjiang Upstream watersheds around Yingxiu Town were selected. First, the landslide-damaged vegetation was identified and monitored via multi-temporal (2001–2014) satellite images. Then, the slope materials stability was assessed through topographic analysis of the vegetation survival environments. Then, the hydrological connectivity index (HCI) was defined to describe the upstream sediment production and downstream transport pathway. Finally, results indicated that HCI decreased annually with the vegetation recovery after the obvious increases during the earthquakes. While, analysis of 2008–2013 debris flow events indicated that the areas, the vertical drop to river < 1000 m and the horizontal distance to river < 2500 m, have high HCI increases and are more susceptible for debris flow formation. Monitoring the landslide-damaged vegetation recovery processes can contribute to assess the hydrological connectivity changes and understand the debris flow formation.

1 Introduction

At 14:28 (Beijng Time, GMT + 8) on 12 May 2008, a devastating mega-earthquake of magnitude 8.0 struck Yingxiu Town of Wenchuan County in Sichuan Province, China (31.0° N and 103.4° E). The earthquake destabilized many mountain slopes causing landslides that damaged large areas of mountain vegetation (Cui et al., 2009; Huang and Li, 2009), and these landslides produced large amounts of loose material (landslide debris) that still deposited on the steep slopes and in the gullies (Tang et al., 2011). And these materials might be directly turned into debris flows or easily en-

NHESSD
3, 1113–1136, 2015

trained by debris flows, whenever a storm of sufficient magnitude occurs (Chen et al., 2009; Tang et al., 2009). Many serious incidents related to debris flows have been reported. On 24 September 2008, a heavy rainstorm in Beichuan County triggered 72 debris-flows (Tang et al., 2009). From 12 to 13 August 2010, 21 debris flows around Qingping town concurrently occurred (Tang et al., 2012). From 13 to 14 August 2010, three regional catastrophic debris-flows occurred near the towns of Gengda, Yingxiu, and Longchi (Xu et al., 2012; Chang et al., 2014). More recently, on 10 July 2013, catastrophic debris-flows occurred in the upper reaches of Minjiang River (Guo et al., 2014).

The combination of steep slope gradients, abundant fragmented surface materials, and high intensity rainfall naturally leads to the catastrophic debris flows in the Wenchuan earthquake-hit area (Cui et al., 2009; Lan et al., 2013; Tang et al., 2009; Xu et al., 2012). Indeed, the earthquake-induced landslides destroyed large areas of vegetation that made the vegetation hydrological adjusting function diminished, and the large amounts of unconsolidated loose materials deposited on the steep slopes that changed the hydrologic progresses (i.e. infiltration reduced, runoff increased and flow concentration expedited) in catchment (Cui et al., 2012). Much research has indicated that the triggering rainfall threshold for debris flows significantly decreased after the earthquake (Cui et al., 2009; Tang et al., 2009; Xu et al., 2012).

This research aims at modeling of slope materials stability and hydrological connectivity changes in one given catchment, and charactering the susceptibility conditions to debris-flow hazards. We selected the Minjiang Upstream watersheds around Yingxiu Town as the study area. First, the earthquake-damaged vegetation was identified and monitored via multi-temporal (2001–2014) satellite images. Then, the slope materials stability was assessed through topographic analysis of the damaged-vegetation survival environments. Then, the hydrological connectivity index (HCI) was defined to describe the upstream sediment production and downstream transport pathway from source to channels/sinks of one reference point in one given catchment. Finally, the HCI changes after the earthquake were detected through monitoring the damaged vegeta-

NHESSD
3, 1113–1136, 2015

tion recovery processes, and the impact of the HCI changes were detected through comparative analysis of 2008–2013 debris flow events.

2 The study area

2.1 The study area location

The study area (625 km^2) is located in the upstream of Minjiang River, near Yingxiu Town, Wenchuan Country, Sichuan, China. It includes four watershed regions; YY watershed, GY watershed, YB watershed, and LX river (Fig. 1). This area was selected for three reasons. First, it is close to the Wenchuan Earthquake epicentre, and was severely affected by the earthquake. Second, the area had rich vegetation before the earthquake, and earthquake-induced landslides damaged large areas of vegetation. Third, multi-temporal (2001–2014) TM/ETM images are available, which can represent the vegetation changes before and after the earthquake.

In addition, the geotectonic movements are active for the complicated fault systems in this region. The Wenchuan earthquake is a result of a sudden rupture of the Yingxiu–Beichuan fault (Dai et al., 2011), which is one part of the Longmenshan thrust belt (Fig. 2). The rocks are primarily comprised of Archean granite, diorite and granodiorite; Sinian andesite; Carboniferous limestone; Trisssic sandstone and Silurian phyllite. Most of bedrocks is deeply fractured and highly weathered, and covered by a layer of weathered material.

2.2 Pre- and post-earthquake vegetation (2001–2014) in the study area

The study area is situated in a subtropical humid monsoon climate zone with an annual average temperature of 12.9 °C, an annual rainfall ranges from 1002 to 1265 mm and approximately 66–76 % of the rain occurs during the rainy season from June to August (Zhang et al., 2012). So, this region was rich with vegetation before the earthquake (Fig. 3).

NHESSD
3, 1113–1136, 2015

The post-earthquake remote sensing images (Fig. 3) show that there are large areas of vegetation were badly damaged by earthquake-induced landslides. And, these areas of damaged vegetation were detected by examining changes in the normalized vegetation index (NDVI) values (Fig. 4). The detail data of the damaged vegetation and recovery conditions was shown in Table 1. Statistical analysis (Table 1) shows that the total size of the damaged area is about 227 km^2, which accounts for 36.3 % of the area of the study area, and each watershed had different damaged conditions. Statistical analysis also indicates that these damaged vegetation areas had recovered by 46.2 % until 2010, and had recovered by 64.2 % until 2014.

3 Methodology

For vegetation influences local capacity to store materials and water and increases infiltration, vegetation contributes towards disconnecting upstream and downstream areas in the mountainous area. Identifying and monitoring the landslide-damaged vegetation can be used to assess the slope material stability and detect the hydrological connectivity changes.

3.1 The slope materials stability susceptibility

The elevation, slope gradient, aspect, distance from the earthquake source and geologic units have been proven to be significant factors for the earthquake-induced landslides (Dai et al., 2011; Huang et al., 2009; Qi et al., 2010; Xu et al., 2013). Hence, the slope materials stability can be assessed through topographic analysis of the vegetation survival environments.

3.1.1 Vegetation growth environments zonation

At the basin (watershed) scale, terrain and lithology control the vegetation growth. Considering that the terrain have natural distribution features in one given basin, the digital

NHESSD
3, 1113–1136, 2015

elevation model (DEM) and slope gradient data were mapped into four classes (1: $< \mu - \sigma$, 2: $[\mu - \sigma, \sigma)$, 3: $[\mu, \mu + \sigma]$, 4: $> \mu + \sigma$) using the mean (μ) and SD (σ) values. And, the slope aspect can be also divided into four classes (1: east, 2: south, 3: west, 4: north) based on the direction of sunshine, too. Furthermore, lithology units can be reclassified into four rock competence (1: high (hard) rocks, 2: high-medium rocks, 3: medium rocks, 4: low (soft) rocks) based on their lithological and structural properties. Hence, one given river basin can be mapped into 256 classes in theory. Each class represents one kind of vegetation growing environments (VGE) and has similar topographical environments and material conditions.

3.1.2 Assessment of the slope materials stability

The vegetation damage probability (VDP) was defined as the ratio of damaged vegetation areas to the total area in each of the VGE regions. And, the vegetative features of each VGE regions are described using NDVI. Then, VDP was used as one initial parameter, and the slope materials stability susceptibility (w) model was trained through multivariate analysis of damaged vegetation and its survival environments as the following function.

$$w = f(d, s, r, v, l) \tag{1}$$

where d is the ratio of the height of the contour above the base (basin mouth) to the total height of the basin, s is the slope gradient, r is the slope aspect, v is the NDVI value, and l is the code for the lithology zonation.

3.2 Hydrological connectivity index model

Mass wasting processes in mountainous terrain are not only dependent on the overall terrain, but also on the spatial organization and the internal connectivity of various topographic units (Borselli et al., 2008; Blahut et al., 2010; Croke et al., 2005; Rogelis et al., 2014). For a given point, mass wasting processes depend on its size of upslope

NHESSD
3, 1113–1136, 2015

source zone and position in the catchment (Fig. 5). We define one hydrological connectivity index (HCI), which includes the upslope (F_u) and downslope (F_d) components, to describe the hydrological connectivity.

$$\mathrm{HCI} = \ln\left(\frac{F_u}{F_d}\right) \tag{2}$$

3.2.1 The upslope component F_u

The upslope component F_u is defined to estimate the upstream sediment production. F_u depends on the topographic conditions (e.g. size, relative relief, and slope gradient) and surface materials of the upslope contributing area. Among these, the topographic factors can be calculated from DEM data, and the material properties can be simplified and expressed as the slope materials stability susceptibility (w). Hence, F_u can be estimated as follows:

$$F_u = a_u \overline{h_u}\,\overline{w_u}\sin(\overline{s_u}) \tag{3}$$

where, a_u, $\overline{h_u}$, $\overline{w_u}$, and $\overline{s_u}$ are the size, average relative altitude, average stability susceptibility, and average slope gradient of the upslope contributing area.

3.2.2 The downslope component F_d

The downslope component F_d is used to describe the transport processes of the upslope sediment. F_d is strongly influenced by the flow pathway conditions, e.g. initial elevation, flow length, slope gradient along pathway, and surface materials along pathway. Hence, the upslope component F_d can be estimated as follows:

$$F_u = \frac{L}{H}\sum_i w_{di}\cos(s_i)C \tag{4}$$

NHESSD
3, 1113–1136, 2015

where, L, H, w_{di}, s_i and C are the horizontal distance to river, vertical drop to river, weighting factor, slope gradient and cell size of the reference point in the give basin. In practice, w_d can be simplified and expressed as $(1 - w_u)$.

4 Results

4.1 The slope materials stability susceptibility at the study area

The study area is mainly underlain by diorite, granite, limestone, and sandstone. All these lithology units belong to the hard rocks. Hence, the vegetation growing environments depend on the topographical conditions mainly, and the each watershed was zoned into 64 kinds of VGE regions basing on the DEM data (Fig. 6). Statistical results indicated that most of VGE regions have similar topographic conditions (e.g. relative relief changes within 200 m, slope gradient changes within 0.13). Then, the slope materials stability susceptibility (w) model was trained and shown in Fig. 6. Finally, these models in the YY, GY, YB watershed and LX river can be expressed as the following functions.

$$w = -0.654d + 1.004\sin(s) + 0.142\sin\left(\frac{r}{2}\right) - 0.131v, \quad R^2 = 0.896 \tag{5}$$

$$w = -0.619d + 1.144\sin(s) - 0.043\sin\left(\frac{r}{2}\right) - 0.056v, \quad R^2 = 0.816 \tag{6}$$

$$w = 0.140d + 0.782\sin(s) - 0.081\sin\left(\frac{r}{2}\right) - 0.234v, \quad R^2 = 0.796 \tag{7}$$

$$w = -0.116d + 0.625\sin(s) + 0.048\sin\left(\frac{r}{2}\right) - 0.219v, \quad R^2 = 0.756 \tag{8}$$

4.2 Hydrological connectivity changes at the study area

Using the TauDEM toolbox in ArcGIS 9.3 platform, both upslope hydrological maps (i.e. flow accumlation, average slope gradient and relative relief of the upslope contributuing

NHESSD
3, 1113–1136, 2015

area) and downslope hydrological maps (i.e. vertical drop to river H, horizontal distance to river L) were calculated and shown in the Fig. 7 using the D-Infinity flow model (Tarboton, 1997).

Then, the study area was divided into vegetation-covered and bare areas, the slope materials stability of the vegetation-covered areas were calculated basing on the multi-temproal NDVI images, and the bare areas were regarded as 1. Finally, pre-earthquake and post-earthquake HCI maps were calculated and shown in Fig. 8. Results showed that the high HCI values are zonally distributed along both sides of the river, especially in YY and GY watersheds.

For further analysis, the multi-temporal HCI changes with H and L was shown in Fig. 9. Statistical results indicated that the areas with $H < 1000$ m have obvious HCI increases (> 0.25), which accounts for 62.7 % of the total areas, the areas with $L < 2500$ m have obvious increases (> 0.25), which accounts for 40.2 % of the total areas, the areas with $H < 1000$ m and $L < 2500$ m have obvious increases (> 0.35), which accounts for 34.9 % of the total areas, and HCI values have slowly decreases and no obvious changing trends with L and H.

Since the earthquake, the study area had suffered severe debris-flow events (Fig. 8). Statistical results showed that the areas with $H < 1000$ m and $L < 2500$ m account for about > 35 % of each debris flow gully area, and these areas have about obvious HCI increases and slower decreases with vegetation recovery. Therefore, we consider that the areas with $H < 1000$ m and $L < 2500$ m, hereafter called the "susceptible areas for debris flow formation, SADFF ", are more susceptible to the debris flow formation, and if the SADFF account more than 35 % of the total gully area, the gully has high potential for debris flow in the wet season.

NHESSD
3, 1113–1136, 2015

5 Discussion

5.1 The assessment of slope materials stability in the study area

To assess the slope materials stability, we deem that the earthquake damaged vegetation areas in one given environment are proportional to its surface materials stability within the same seismic intensity conditions. Hence, there are two main limitations on its application: (1) the study area was covered by vegetation, and under the similar climate conditions, (2) the study area was struck by the earthquake that had high magnitude and strong destructive force, and is situated in the zone with the same seismic intensity level.

5.2 The impact of the hydrological connectivity changes after the earthquake

Guo et al. (2014) found that the lowest rainfall intensity and rainfall amount for debris flow initiation rise up annually through analysis in the study area. We collected some rainfall records during 2010–2013 debris flow events, and the triggering rainfall intensity (TRI) for debris flow initiation ($mm\,h^{-1}$), the early effective rainfall (EER), the accumulative rainfall with a period of 6 h (ARC6) and with a period of 12 h (ARC12) before debris flow occurred (mm) of these rainfall records were shown in Table 2. The HCI values in SADFF areas from 2007 to 2014 were shown in Table 2, too. The results indicated that the high rainfall intensity can easily trigger the debris flows, and the debris flow formation in the gully with low HCI need high EER, ARC6 and ARC12. Therefore, HCI analysis can provide some information for understanding the rainfall conditions of debris flow, but it is still challenging to predict the precise rainfall conditions of debris flow events.

NHESSD
3, 1113–1136, 2015

6 Conclusions

Since 2008, the earthquake-damaged vegetation has been recovering. Importantly, the recovery vegetation helps to stabilize slope materials and adjust hydrological processes. The conditions of the debris flow initiation have changed with the damaged vegetation recovery.

We identify and monitor the landslide-damaged vegetation and its recovery processes via multi-temporal (2001–2014) satellite images, and monitoring results indicate that these damaged vegetation areas about 227 km^2, which accounts for 36.3 % of the area of the study area, and these damaged vegetation areas had recovered by 46.2 % until 2010, and had recovered by 64.2 % until 2014. We consider that these vegetation recovered areas returned to its geomorphic equilibrium within a few years, possibly because most of the landslides were a shallow type and because of rapid growth of vegetation that helped stabilize the slopes.

We model hydrological connectivity index (HCI) to detect the hydrologic processes changes with the landslide-damaged vegetation recovery, and the HCI results indicated that HCI obviously increased after the earthquake, and HCI decreased annually with the vegetation recovery. We consider that the lowest rainfall intensity and rainfall amount for debris flow initiation would rise up annually with HCI decreases and vegetation recovery. In additions, we fund that the areas ($H < 1000$ m and the $L < 2500$ m) have high HCI increases and are susceptible for debris flow formation in the study area.

Acknowledgements. This research was financially supported by the National Science and Technology Support Program (No. 2012BAC06B02), the key Projects of the Chinese Academy of Sciences (No. KZZD-EW-05-01-04), and the Beijing Natural Science Foundation (No. 4144088).

NHESSD
3, 1113–1136, 2015

References

Blahut, J., Horton, P., Sterlacchini, S., and Jaboyedoff, M.: Debris flow hazard modelling on medium scale: Valtellina di Tirano, Italy, Nat. Hazards Earth Syst. Sci., 10, 2379–2390, doi:10.5194/nhess-10-2379-2010, 2010.

Borselli, L., Cassi, P., and Torri, D.: Prolegomena to sediment and flow connectivity in the landscape: a GIS and field numerical assessment, Catena, 75, 268–277, doi:10.1016/j.catena.2008.07.006, 2008.

Chang, M., Tang, C., Zhang, D.-D., and Ma, G.-C.: Debris flow susceptibility assessment using a probabilistic approach: a case study in the Longchi area, Sichuan province, China, J. Mt. Sci., 11, 1001–1014, doi:10.1007/s11629-013-2747-9, 2014.

Chen, N., Yang, C., Zhou, W., Hu, G., Li, H., and Hand, D.: The critical rainfall characteristics for torrents and debris flows in the Wenchuan earthquake stricken area, J. Mt. Sci., 6, 362–372, doi:10.1007/s11629-009-1064-9, 2009.

Croke, J., Mockler, S., Fogarty, P., and Takken, I.: Sediment concentration changes in runoff pathways from a forest road network and the resultant spatial pattern of catchment connectivity, Geomorphology, 68, 257–268, doi:10.1016/j.geomorph.2004.11.020, 2005.

Cui, P., Chen, X., Zhu, Y., Su, F., Wei, F., Han, Y., Liu, H., and Zhuang, J.: The Wenchuan Earthquake (May 12, 2008), Sichuan Province, China, and resulting geohazards, Nat. Hazards, 56, 19–36, doi:10.1007/s11069-009-9392-1, 2009.

Cui, P., Lin, Y., and Chen, C.: Destruction of vegetation due to geo-hazards and its environmental impacts in the Wenchuan earthquake areas, Ecol. Eng., 44, 61–69, doi:10.1016/j.ecoleng.2012.03.012, 2012.

Dai, F. C., Xu, C., Yao, X., Xu, L., Tu, X. B., and Gong, Q. M.: Spatial distribution of landslides triggered by the 2008 Ms 8.0 Wenchuan earthquake, China, J. Asian Earth Sci., 40, 883–895, doi:10.1016/j.jseaes.2010.04.010, 2011.

Guo, X., Cui, P., Ma, L., and Kong, Y.: Triggering rainfall characteristics for debris flows along Dujiangyan–Wenchuan highway of Sichuan, Mount. Res., 6, 736–346, 2014.

Huang, R. and Li, W.: Development and distribution of geohazards triggered by the 5.12 Wenchuan Earthquake in China, Sci. China Ser. E, 52, 810–819, doi:10.1007/s11431-009-0117-1, 2009.

NHESSD
3, 1113–1136, 2015

Lan, H. X., Li, L. P., Zhang, Y. S., Gao, X., and Liu, H. J.: Risk assessment of debris flow in Yushu seismic area in China: a perspective for the reconstruction, Nat. Hazards Earth Syst. Sci., 13, 2957–2968, doi:10.5194/nhess-13-2957-2013, 2013.

Qi, S., Xu, Q., Lan, H., Zhang, B., and Liu, J.: Spatial distribution analysis of landslides triggered by 2008.5.12 Wenchuan Earthquake, China, Eng. Geol. , 116, 95–108, doi:10.1016/j.enggeo.2010.07.011, 2010.

Rogelis, M. C. and Werner, M.: Regional debris flow susceptibility analysis in mountainous periurban areas through morphometric and land cover indicators, Nat. Hazards Earth Syst. Sci., 14, 3043–3064, doi:10.5194/nhess-14-3043-2014, 2014.

Tang, C., Zhu, J., Li, W. L., and Liang, J. T.: Rainfall-triggered debris flows following the Wenchuan earthquake, B. Eng. Geol. Environ., 68, 187–194, doi:10.1007/s10064-009-0201-6, 2009.

Tang, C., Zhu, J., Ding, J., Cui, X. F., Chen, L., and Zhang, J. S.: Catastrophic debris flows triggered by a 14 August 2010 rainfall at the epicenter of the Wenchuan earthquake, Landslides, 8, 485–497, doi:10.1007/s10346-011-0269-5, 2011.

Tang, C., van Asch, T. W. J., Chang, M., Chen, G. Q., Zhao, X. H., and Huang, X. C.: Catastrophic debris flows on 13 August 2010 in the Qingping area, southwestern China: the combined effects of a strong earthquake and subsequent rainstorms, Geomorphology, 139–140, 559–576, doi:10.1016/j.geomorph.2011.12.021, 2012.

Tarboton, D. G.: A new method for the determination of flow directions and upslope areas in grid digital elevation models, Water Resour. Res., 33, 309–319, doi:10.1029/96wr03137, 1997.

Xu, C., Xu, X., Yao, X., and Dai, F.: Three (nearly) complete inventories of landslides triggered by the May 12, 2008 Wenchuan Mw 7.9 earthquake of China and their spatial distribution statistical analysis, Landslides, 11, 441–461, doi:10.1007/s10346-013-0404-6, 2013.

Xu, Q., Zhang, S., Li, W. L., and van Asch, Th. W. J.: The 13 August 2010 catastrophic debris flows after the 2008 Wenchuan earthquake, China, Nat. Hazards Earth Syst. Sci., 12, 201–216, doi:10.5194/nhess-12-201-2012, 2012.

Zhang, S., Zhang, L. M., Peng, M., Zhang, L. L., Zhao, H. F., and Chen, H. X.: Assessment of risks of loose landslide deposits formed by the 2008 Wenchuan earthquake, Nat. Hazards Earth Syst. Sci., 12, 1381–1392, doi:10.5194/nhess-12-1381-2012, 2012.

NHESSD

3, 1113–1136, 2015

Table 1. Statistical data of damaged vegetation and recovery conditions from 2008 to 2014.

Watershed code	Area (km^2)	Damaged vegetation (km^2)		Recovered vegetation (km^2)	
		18 Jul 2008	3 Jun 2009	18 Mar 2010	1–17 Jun 2014
LX river	78.7	12.2	10.3	5.1	8.3
YB	79.3	16.4	15.4	5.4	11.5
YY	316.7	127.7	122.7	61.1	82.4
GY	150.6	70.5	68.8	33.1	43.4
Total	625.3	226.8	217.2	104.7	145.6

NHESSD
3, 1113–1136, 2015

Table 2. Triggering rainfall characteristics for the debris flow events with HCI changes from 2010 to 2013.

Gully	Date	Rainfall characteristics				HCI changes features			
		TRI	EER	ARC6	ARC12	2007	2008	2009	2014
Baiyi gully	13 Aug 2010	53.5	41.1	0.5	40.7	−0.34	0.12	0.13	−0.09
Hongchun gully	14 Aug 2010	16.4	162.1	45.0	94.5	1.62	2.14	2.09	1.85
Hongchun gully	21 Aug 2011	56.5	145.0	–	–	1.62	2.14	2.09	1.85
Niujuan gully	3 Jul 2011	27.1	46.7	18.7	41.0	1.32	1.78	1.76	1.53
Gaojia gully	3 Jul 2011	34.4	100.8	80.8	92.1	1.17	1.60	1.56	1.32
Taoguan gully	9 Jul 2013	18.6	126.4	37.5	49.8	0.54	0.96	0.91	0.75
Guxi gully	9 Jul 2013	17.1	192.5	51.8	71.0	0.42	0.81	0.79	0.62

NHESSD
3, 1113–1136, 2015

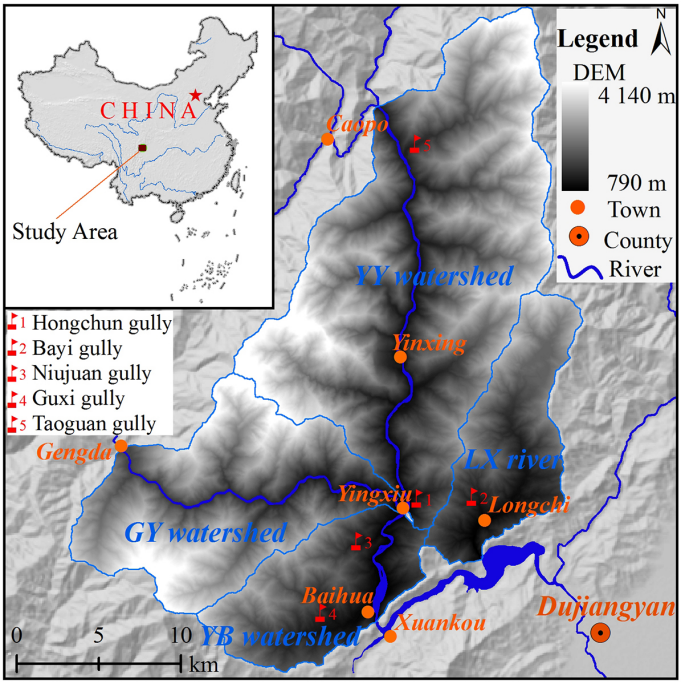

Figure 1. Location of the study area (from the Columbus Navigation Homepage).

NHESSD
3, 1113–1136, 2015

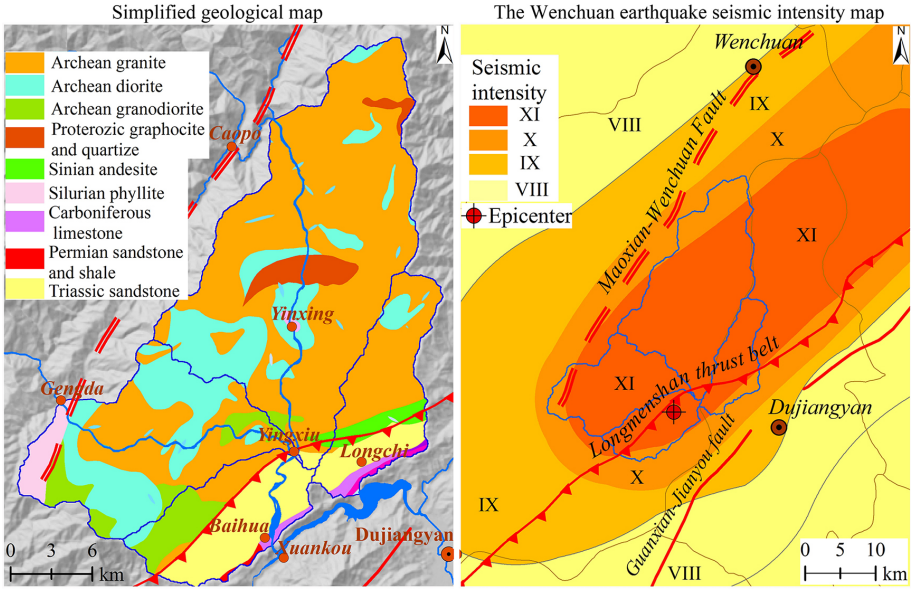

Figure 2. Geological settings and the Wenchuan earthquake seismic intensity maps at the study area.

NHESSD
3, 1113–1136, 2015

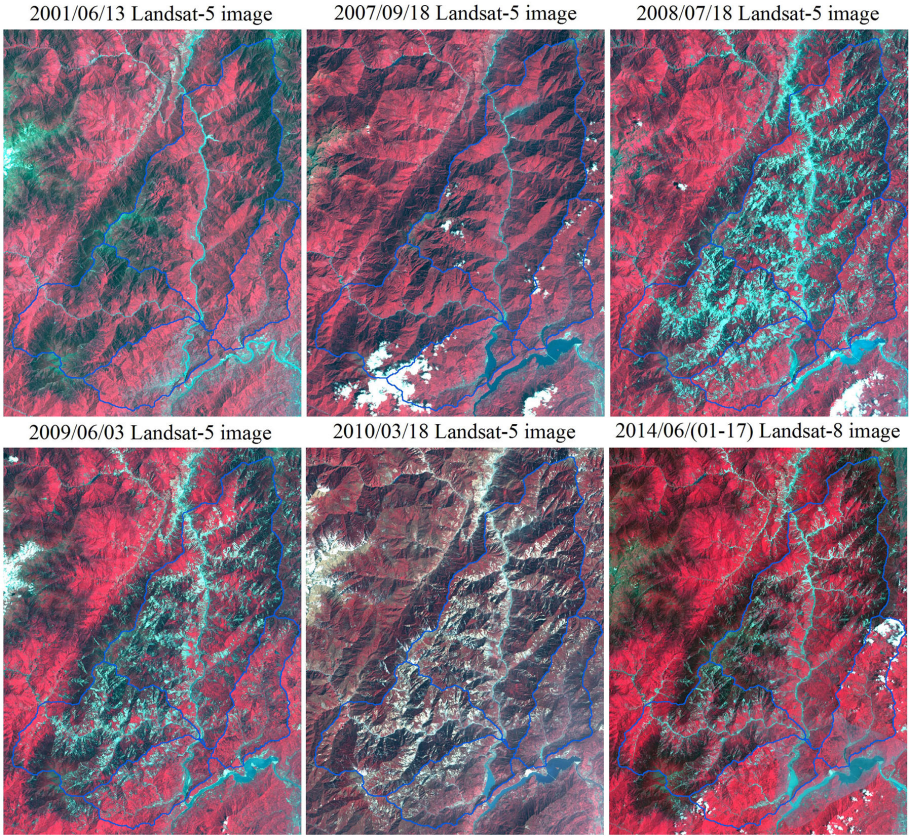

Figure 3. Landsat-5/8 (2001–2014) images at the study area.

NHESSD
3, 1113–1136, 2015

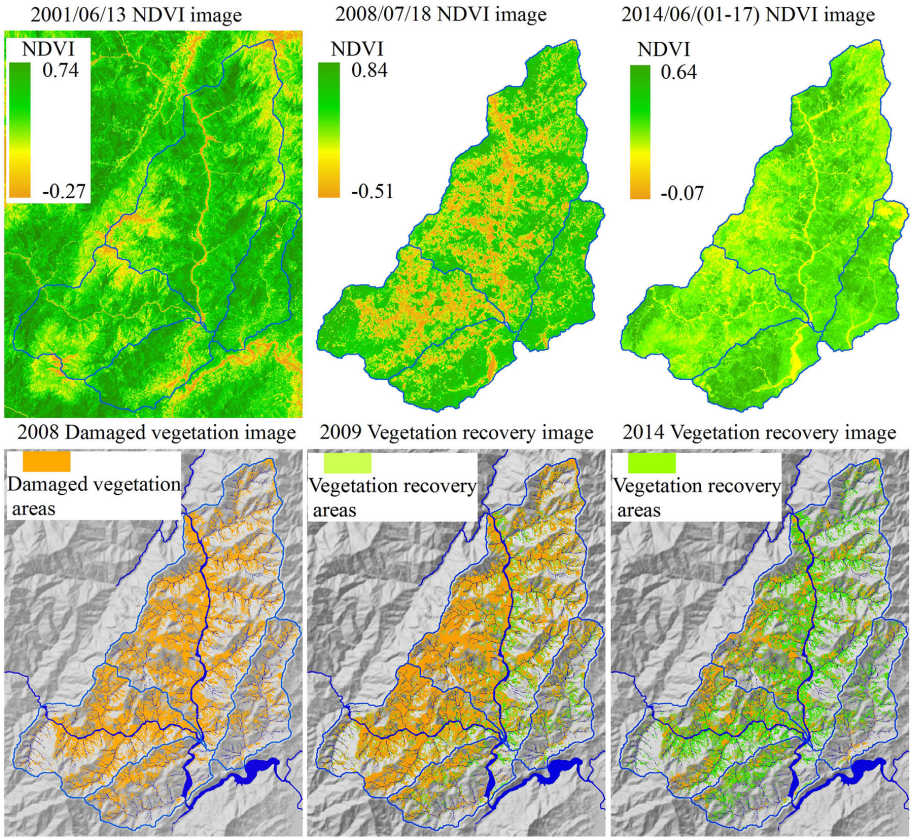

Figure 4. Landsat-5/8 (2001–2014) NDVI images, damaged vegetation and its post-earthquake recovery images at the study area.

NHESSD
3, 1113–1136, 2015

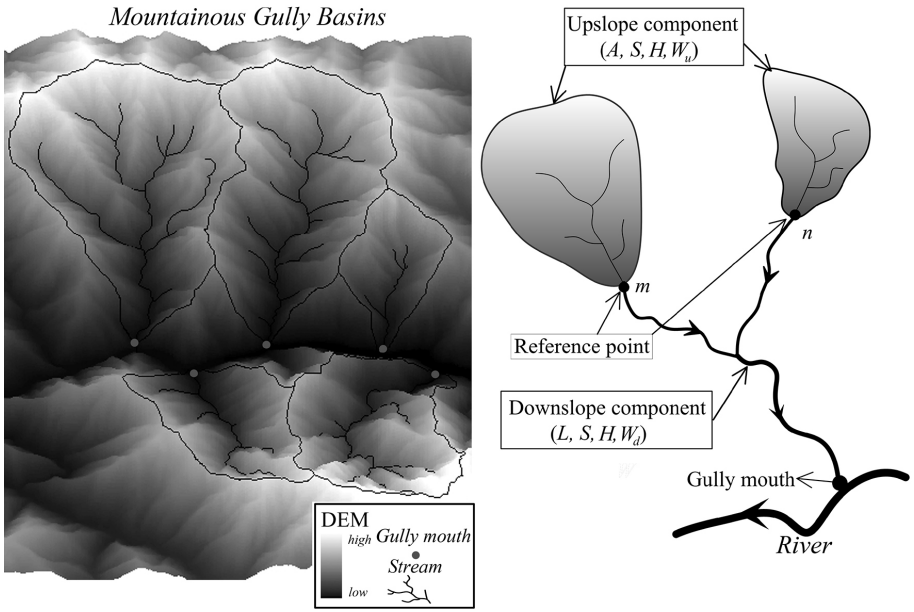

Figure 5. Hydrological conditions of mountainous gully basins.

NHESSD
3, 1113–1136, 2015

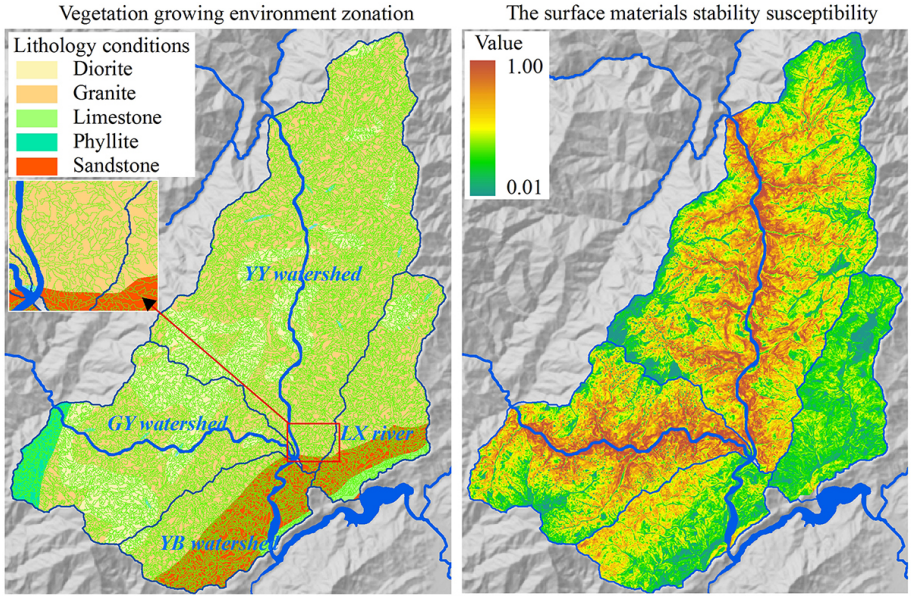

Figure 6. Vegetation growing environment zonation and the surface materials stability susceptibility at the study area.

NHESSD
3, 1113–1136, 2015

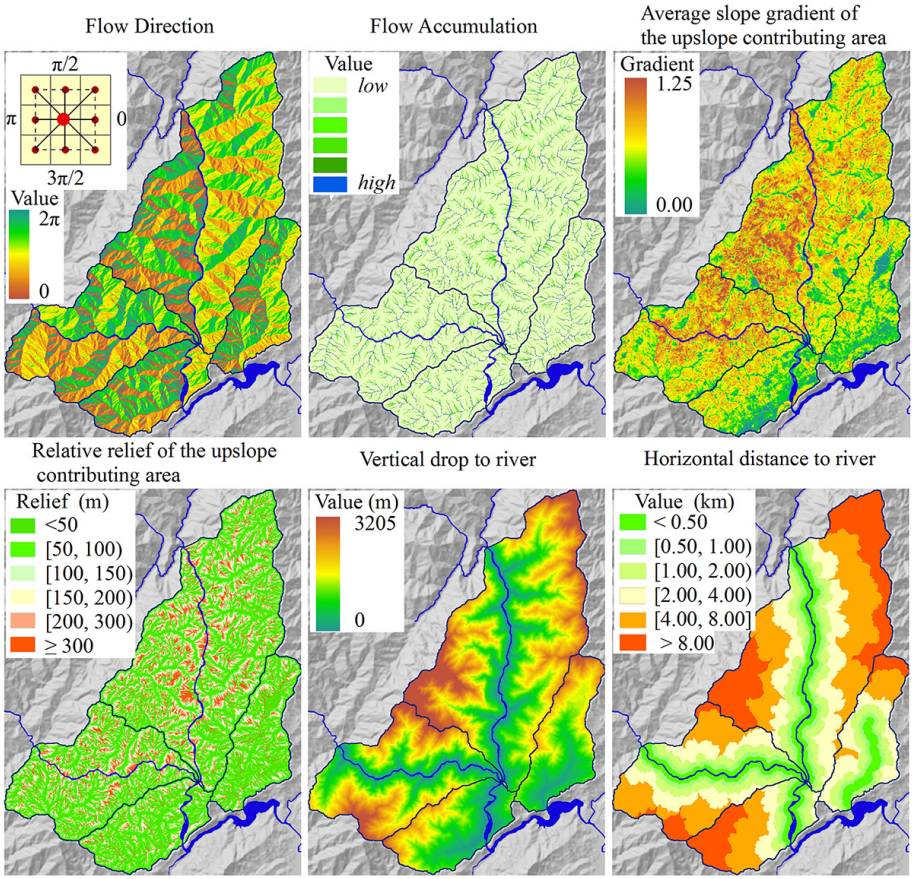

Figure 7. Hydrological analysis of the study area.

NHESSD
3, 1113–1136, 2015

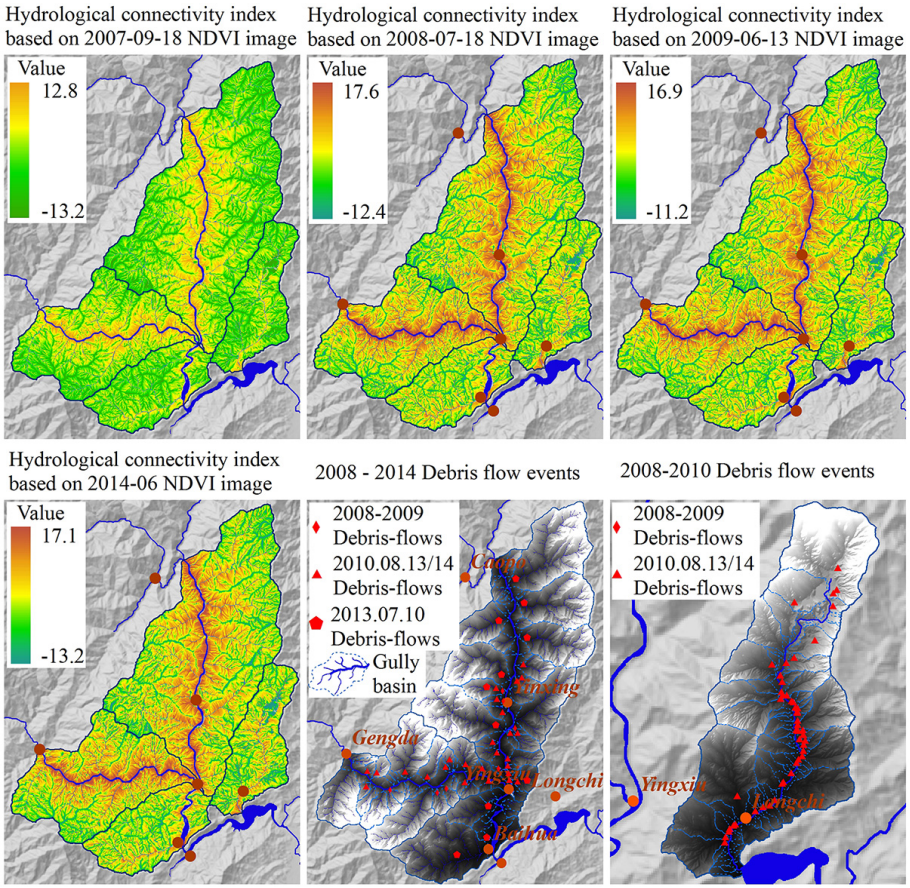

Figure 8. The hydrological connectivity index map and the 2008–2013 debris-flow events at the study area.

NHESSD
3, 1113–1136, 2015

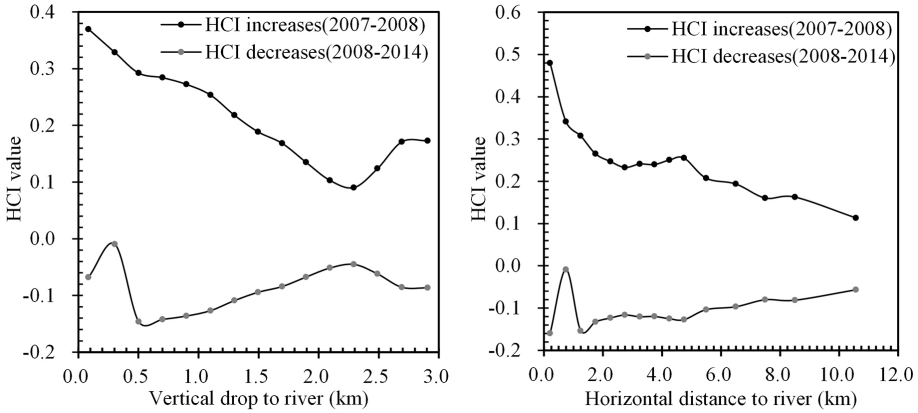

Figure 9. Statistical reseults of hydrological connectivity change processes from 2007 to 2014.

NHESSD
3, 1113–1136, 2015